CANDIDACY PAPER
May 5, 1999

W^+W^- Production at the Large Electron Positron Collider.

B. Vachon
University of Victoria

Abstract

The study of W pair events at the Large Electron Positron collider is reviewed. A discussion of how W^+W^- events are produced and identified in the OPAL detector is presented. The techniques used to measure the W^+W^- cross-section, W branching fractions and the mass of the W boson are summarized. An overview of triple gauge couplings and their sensitivity to new physics is also included.

Introduction

The Standard Model of particle physics is a successful theory describing the interactions between fundamental particles [1]. It however contains many free parameters, such as the couplings and masses of the particles, that must be experimentally measured. Precision measurements of many of these parameters have been made and can be used to evaluate other unknown parameters or to put limits on new physics beyond the Standard Model.

This report focuses on the measurements of the W boson properties using W pair events (W^+W^-) produced via the $e^+e^- \to W^+W^-$ reaction[1]. The W boson is the particle mediating the charged weak force. Precision measurements of the mass of the W can be used to place limits on the mass of the hypothetical Higgs particle. In addition, the reaction producing W^+W^- events involves the interaction between three spin 1 particle: γW^+W^- and $Z^0W^+W^-$. A study of the structure of these interactions can be used to search for new physics.

W pair events are produced at the Large Electron Positron (LEP) collider located just outside Geneva. The results presented in this report were obtained using W^+W^- events observed by the OPAL (Omni-Purpose Apparatus at LEP) detector[2]. Since 1996, LEP has been colliding electrons and positrons at a centre-of-mass energy above 161 GeV where it is kinematically possible to produce pairs of W bosons[3]. Prior to 1996, W bosons were only produced at proton-antiproton colliders. Measurements of the W boson properties at proton-antiproton colliders complement the results obtained at LEP. The details of the measurements performed at proton-antiproton colliders will not be described in this report but their results will be compared to LEP measurements when possible.

The first two sections of the report contain a brief introduction to the Standard Model and a discussion of how W^+W^- events are produced and identified using the OPAL detector. Section 3 describes the measurements of the W boson properties. The couplings between three spin 1 particles (γW^+W^- or $Z^0W^+W^-$) and their sensitivity to new physics are presented in section 4. Finally, a summary of this report is presented in Section 5.

1 Standard Model

The Standard Model (SM) of particle physics describes the interactions between fundamental particles [4]: leptons, quarks and gauge bosons. For each lepton and quark there exists a corresponding anti-particle with the same mass. Anti-particles have quantum numbers that are the negative of the ones given to particles. Leptons and quarks are particles with half-integer spin (fermions) and can be classified in three categories referred to as generations or families (see Table 1). Within each generation, leptons and quarks are arranged in doublets. These doublets of particles are based on the preference of the charged weak force

[1] A positron (e^+) is the anti-particle of the electron.

[2] There are four detectors at the LEP collider: ALEPH, DELPHI, L3 and OPAL.

[3] To produce two W bosons, conservation of energy requires that the energy available be at least equal to the sum of the mass of the two W bosons (80 GeV + 80 GeV $\approx$ 160 GeV).

[4] Fundamental particles are believed to be indivisible and to form the building blocks of all matter.

	First Generation	Second Generation	Third Generation	Electric Charge (e)
Leptons	$\begin{pmatrix} e^- \\ \nu_e \end{pmatrix}$	$\begin{pmatrix} \mu^- \\ \nu_\mu \end{pmatrix}$	$\begin{pmatrix} \tau^- \\ \nu_\tau \end{pmatrix}$	-1 0
Quarks	$\begin{pmatrix} u \\ d \end{pmatrix}$	$\begin{pmatrix} c \\ s \end{pmatrix}$	$\begin{pmatrix} t \\ b \end{pmatrix}$	$+2/3$ $-1/3$

Table 1: Leptons and quarks arranged in three generations. The electric charge of the particles is listed in the last column in units of the electron charge.

to couple members of a same doublet. The quark doublets observed in nature are slightly more complicated. They are a linear combination of the mass states given in Table 1.

There are four fundamental forces in nature: gravitational, weak, electromagnetic and strong forces. Interactions between particles are described, in quantum field theory, in terms of the exchange of field particles with integer spin called mediators or gauge bosons. The mediators of each force are listed in Table 2. Neutrinos (ν) are neutral particles that interact only weakly with matter. Charged leptons participate in the weak and electromagnetic forces. Quarks, in addition to the electromagnetic and weak forces, also interact through the strong force. Composite particles made of quarks are called hadrons. Isolated quarks are not found due to the nature of the strong force. The strong force increases with distance. Therefore, when two quarks are pulled apart, the potential energy becomes so large that new quark-antiquark pairs are produced an combine to form new hadrons in a process called hadronization. At high energy, this results in collimated jets of hadrons.

Force	Mediator
Gravitational	Graviton
Weak	W^+, W^- and Z^0
Electromagnetic	Photon (γ)
Strong	Gluon (g)

Table 2: The four fundamental forces in nature and the particles mediating the forces. Note that the graviton has not been experimentally observed.

The charged mediator of the weak force, the W boson, was discovered in 1983 at the CERN SPS Proton-Antiproton Collider in Geneva [2]. The properties of the W boson have more recently been studied at the LEP collider at CERN and at the proton-antiproton collider at Fermilab in Chicago. The W boson has a mass of roughly 80 GeV, approximately 160 000 times heavier than an electron. It has an extremely short lifetime of the order of 10^{-25} seconds. The W may decay into each of the doublets given in Table 1. The W boson

decays to two leptons 32.2% of the time ($W \to l\bar{\nu}_l$)[5]. It can also decay hadronically 67.8% of the time ($W \to q\bar{q}$) [3]. It is very difficult to identify the flavour of the quarks since only secondary hadrons are observed in the detector. The W boson cannot decay to a doublet composed of a top and bottom quark since the top quark is heavier than the W boson.

Unlike the other gauge bosons, the mediators of the weak force (W^+, W^-, Z^0) are massive particles. In the SM, their masses can be theoretically explained by the "Higgs mechanism" [4]. This mechanism is built on the concept of local gauge invariance and symmetry breaking of a Lagrangian density describing the dynamics of a scalar field. As a result of the "Higgs mechanism", the W and Z^0 bosons acquire mass and a massive scalar particle appears in the interaction Lagrangian. This new particle is called a Higgs and has not yet been experimentally observed.

A precision measurement of the W boson mass (M_W) can be used to set limits on the mass of the Higgs (M_H). In the Standard Model, the mass of the W boson is predicted to be [5]

$$M_W = \left(\frac{\pi\alpha_{(M_Z^2)}}{\sqrt{2}G_F}\right)^{1/2} \frac{1}{\sin\theta_w\sqrt{1-\Delta r}}$$

where G_F is the Fermi constant, $\alpha_{(M_Z^2)}$ is the electromagnetic coupling constant evaluated at the Z^0 mass and θ_w is the weak mixing angle. All these parameters can be measured experimentally to determine the size of the radiative corrections Δr. The dominant contributions to Δr depend on the top quark and the Higgs masses [6]. The mass of the top quark has been measured at the Fermilab proton-antiproton collider, hence an improvement in the precision of M_W will give a better constraint on the Higgs mass.

2 W^+W^- Production

Interactions in physics can be represented using Feynman diagrams. These diagrams are purely symbolic and do not represent by any means the trajectories of the particles. In momentum-space, the interactions between particles can be express as a perturbation series in terms of the couplings between particles. Each term in the series corresponds to a particular Feynman diagram. Diagrams representing first-order terms are called "tree level" diagrams. Figure 1 shows the tree level Feynman diagrams for the production of W^+W^- bosons.

Diagrams (a) and (b) contain a vertex involving three gauge bosons. The couplings associated with these vertices are usually referred to as Triple Gauge Couplings (TGCs). A discussion of TGCs is presented in Section 4. Diagram (c) represents the scattering of an electron (e^-) and a positron (e^+) via the exchange of an electron neutrino (ν_e).

The presence of a fourth tree-level diagram is possible if the Higgs particle exists. This fourth diagram would be equivalent to diagrams (a) and (b) where the γ or Z^0 is replaced by a neutral Higgs (H^0). Since the coupling to the Higgs is theoretically proportional to the mass of the interacting particles, this fourth diagram would be greatly suppressed due

[5]Charge conjugation is assumed throughout this paper, i.e. W^+ is assumed to have the same properties as W^-. The leptonic decay $W \to l\bar{\nu}_l$ implicitly refers to $W^+ \to l^+\nu_l$ or $W^- \to l^-\bar{\nu}_l$.

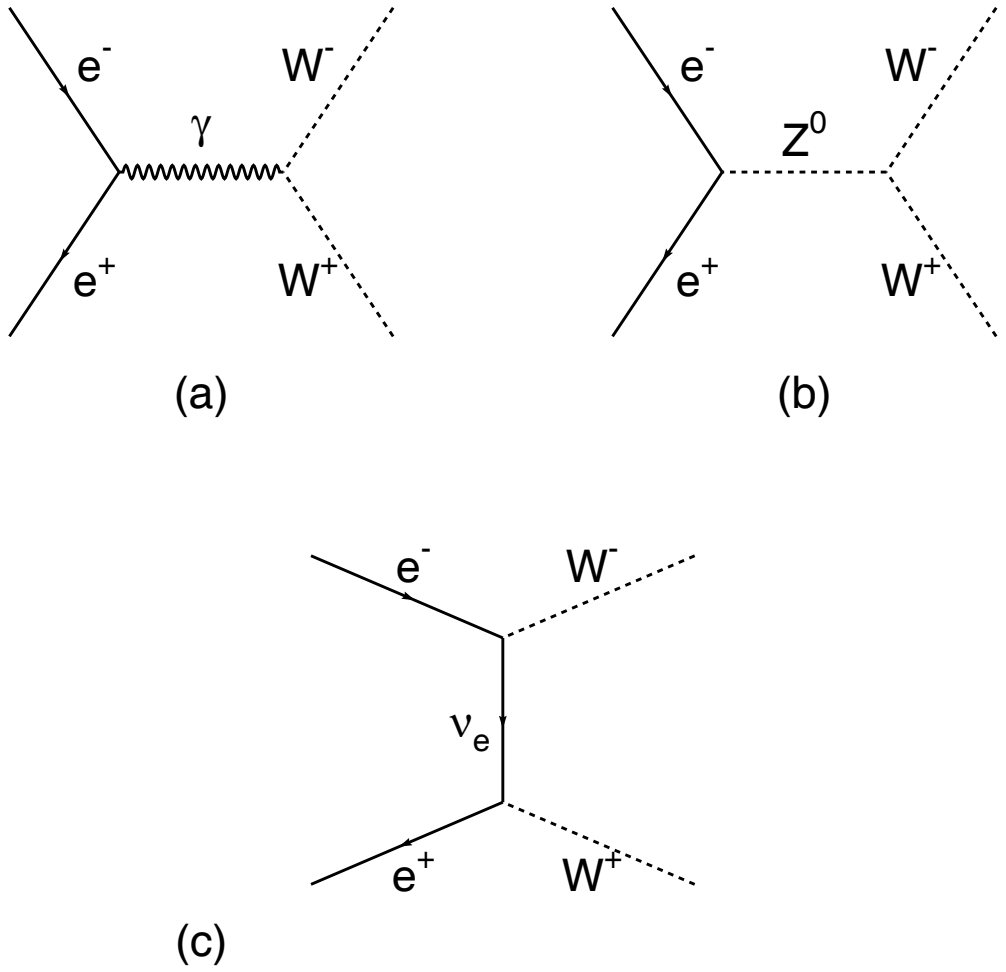

Figure 1: Tree level Feynman diagrams representing the production of W^+W^- from an electron and a positron. Diagrams (a) and (b) contain a vertex between three gauge bosons (γW^+W^- and $Z^0W^+W^-$ respectively).

to the small mass of the electron (positron). Even if the Higgs particle exists, it would not significantly modify the values of Triple Gauge Couplings within the current experimental precision. Thus, the production of W^+W^- bosons from a Higgs is ignored throughout this report.

2.1 Identification of W^+W^- events.

W bosons can decay into lepton or quark doublets as discussed in section 1. The possible final states of a W^+W^- event can therefore be: $W^+W^- \to \bar{l}\nu_l l'\bar{\nu}_{l'}$, where each W decays to two leptons, $W^+W^- \to q\bar{q}q'\bar{q}'$, where each W decays to two quarks or $W^+W^- \to q\bar{q}\bar{l}\nu_l$, where one W decays leptonically and one W decays hadronically[6] .

Each final state has a particular experimental "signature" in the OPAL detector. A detailed description of the OPAL detector can be found in [7]. Figure 2 shows a reconstruction of a typical W^+W^- event for each possible final state. Each picture represents a cross-sectional view of the OPAL detector where the direction of the beam points out of the page. The trajectories of charged particles in the central drift chamber are represented by solid lines. The yellow (pink) boxes represent the amount of energy deposited in the electromagnetic (hadronic) calorimeter of the OPAL detector. The size of the boxes is proportional to the amount of energy deposited.

$W^+W^- \to \bar{l}\nu_l l'\bar{\nu}_{l'}$ events are characterized by an acoplanar[7] pair of charged leptons. The total momentum of the event does not appear to be conserved due to the presence of two undetected neutrinos. Background to $W^+W^- \to \bar{l}\nu_l l'\bar{\nu}_{l'}$ events mainly comes from four-fermion production processes such as $e^+e^- \to Z^0Z^0$ and $e^+e^- \to We\bar{\nu}_e$.

$W^+W^- \to q\bar{q}\bar{l}\nu_l$ events have two hadronic jets, one high momentum lepton and some missing momentum due to the presence of a neutrino. The selected sample of $W^+W^- \to q\bar{q}\bar{l}\nu_l$ events is predominantly contaminated by four-fermion processes such as $e^+e^- \to Z^0Z^0$, $e^+e^- \to We\bar{\nu}_e$ and $e^+e^- \to Z^0e^+e^-$ which can lead to two hadronic jets and one identified lepton being observed in the detector. The process producing two fermions via $e^+e^- \to Z^0/\gamma \to q\bar{q}$ where a hadron or radiated photon is misidentified as a lepton is also a source of background for $W^+W^- \to q\bar{q}\bar{l}\nu_l$ events

Finally, $W^+W^- \to q\bar{q}q'\bar{q}'$ events contain four jets of particles. Since no neutrinos are produced from the decays of the W bosons, the event has no significant missing momentum. The sample of candidate $W^+W^- \to q\bar{q}q'\bar{q}'$ events is mainly contaminated by events coming from the reaction $e^+e^- \to Z^0/\gamma \to q\bar{q}$ associated with radiated energetic photons or with gluon radiation producing a total of four jets.

[6]The symbol $q\bar{q}$ implicitly refers to any doublet of quarks that can be produced from a W decay. Similarly, $l\bar{\nu}_l$ refers to any doublet of leptons including charge conjugate modes. The symbol ' is used to explicitly indicate that both W bosons do not have to decay to the same leptons or quarks final states.

[7]By convention, acoplanar means particles not produced in the same plane with respect to the r-ϕ coordinates of the detector, i.e. particles are not back to back in the r-ϕ plane. The electron beam is defined as the z-axis of the detector.

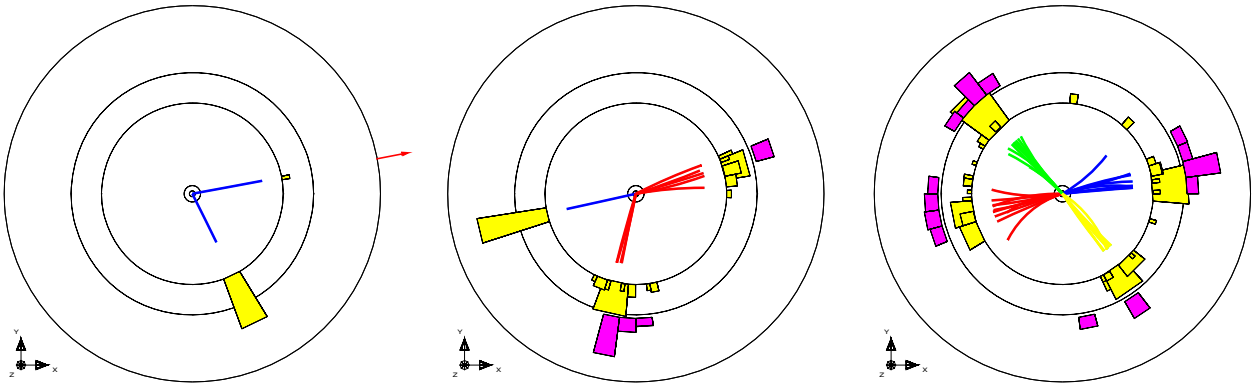

$W^+W^- \to \bar{l}\nu_l l'\bar{\nu}_{l'}$ $W^+W^- \to q\bar{q}\bar{l}\nu_l$ $W^+W^- \to q\bar{q}q'\bar{q}'$

Figure 2: Reconstruction of typical events for each possible W^+W^- final state. The picture represents a cross-sectional view of the OPAL detector where the direction of the beam points out of the page. The solid lines represent the tracks of charged particles in the central drift chamber. The yellow (pink) boxes represent the amount of energy deposited in the electromagnetic (hadronic) calorimeter of the OPAL detector. The size of the yellow (pink) boxes is proportional to the amount of energy deposited. The red arrows indicate hits in the muon chambers of the detector. The first picture (left) represents a W^+W^- event in which one W decayed to an electron and electron neutrino and one W decayed to a muon and muon neutrino. In the middle picture, one W decayed hadronically forming two jets of particles and the other W decayed to an electron and an electron neutrino. The last picture (right) represents an event in which each W has decayed hadronically forming four jets of particles.

2.2 Data Sample

The cross-section of the $e^+e^- \to$ hadrons reaction is shown as function of the centre-of-mass energy ($\sqrt{s}$) in Figure 3. At low energy, the cross-section is proportional to $1/s$ due to the photon annihilation diagram ($e^+e^- \to \gamma \to$ hadrons). A significant enhancement of the cross-section is present at a centre-of-mass energy close to the Z^0 mass ($\sim$ 90 GeV) where hadrons can be produced via a Z^0. Above 161 GeV, final state hadrons can be produced from W^+W^- events, resulting in a sudden rise in the cross-section. From 1990-1995, LEP collided electrons and positrons at a centre-of-mass energy close to the Z^0 mass. In 1996, in its second phase of operation (LEP2), LEP has increased its centre-of-mass energy above the W^+W^- production cross-section threshold.

In 1997, LEP operated at a centre-of-mass energy of 183 GeV during which the OPAL detector recorded an integrated luminosity[8] of 57.21$\pm$0.15$\pm$0.20 pb^{-1} where the first error

[8]The luminosity ($\mathcal{L}$) is the number of particles passing in the beam per unit time, per unit area. The integrated luminosity refers to the luminosity integrated over time and is generally expressed in pb^{-1} where 1 pb = 10^{-38}cm^2.

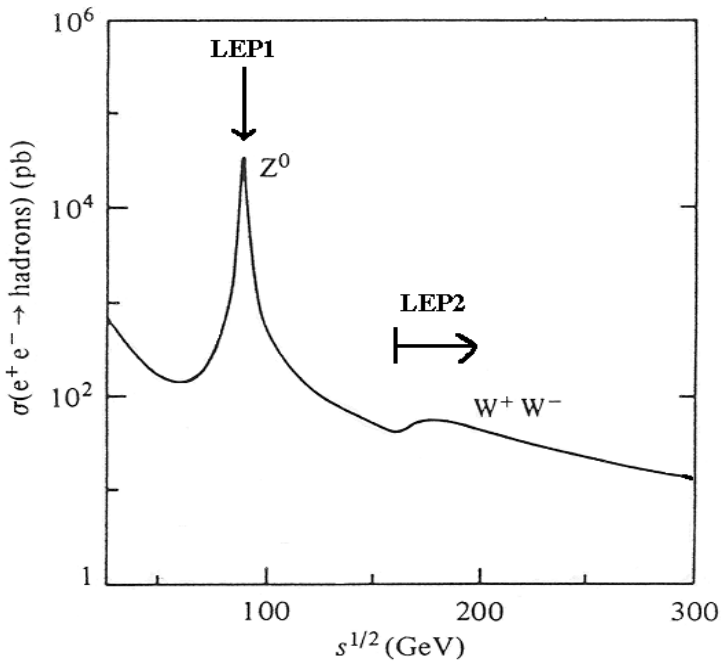

Figure 3: Plot of the SM prediction for the $e^+e^- \to$ hadrons cross-section versus the centre-of-mass energy ($\sqrt{s}$). In the first phase of operation (LEP1), LEP collided electrons and positrons at a centre-of-mass energy close to the Z^0 mass. LEP is now running at a centre-of-mass energy higher than the W^+W^- production threshold.

is statistical and the second systematic [8]. The luminosity $\mathcal{L}$ is measured at OPAL using small angle Bhabha[9] scattering events detected in the forward silicon tungsten calorimeter. The number of events produced in the detector from a particular reaction is equal to the reaction cross-section times the integrated luminosity. The identification of W^+W^- events is not fully efficient and other type of events can pass the W^+W^- selections. Table 3 shows the number of candidate events for each type of W^+W^- decay collected by the OPAL detector at a centre-of-mass energy of 183 GeV [8]. An estimate of the purity and efficiency for selecting events of each decay type is also given.

3 W Boson Properties

3.1 W^+W^- Cross-Section and W Decay Branching Fractions

The W^+W^- production cross-section (σ_{WW}) and W branching fractions[10] (B) are measured by comparing the number of observed and expected W^+W^- events in each possible final state. Table 4 shows the number of observed and expected events as well as the selection

[9]Scattering of an electron and positron through a photon, $e^+e^- \to e^+e^-$.

[10]The fraction of all particles of a given type that decay to a particular final state.

Event Type	Number of Candidates	Selection Efficiency	Purity
$W^+W^- \to \bar{l}\nu_l l'\bar{\nu}_{l'}$	78	78.0%	93.8%
$W^+W^- \to q\bar{q}\bar{l}\nu_l$	361	84.7%	90.2%
$W^+W^- \to q\bar{q}q'\bar{q}'$	438	84.6%	78.3%

Table 3: Number of candidate events of each W^+W^- decay type selected at a centre-of-mass of 183 GeV. an estimate of the purity and efficiency for selecting events of each decay type is also given.

efficiencies for each of the ten possible final states. The expected number of events presented in that Table is calculated assuming a SM W^+W^- cross-section of 15.72 pb at a centre-of-mass energy of 182.68±0.05 GeV and for a W mass of 80.40±0.09 GeV. The W branching fractions are also set to their SM values.

For each of the ten W^+W^- decay types ($i = 1, 10$) shown in Table 4, the expected number of events can be calculated as,

$$\mu_i = \sigma_{WW}\mathcal{L}\sum_{j=1}^{10}\epsilon_{ij}(\mathrm{B}_{W1}\mathrm{B}_{W2})_j \ + \ \mathrm{N}_i^{\mathrm{bkg}} \ .$$

The selection of W^+W^- events of type i also selects, with smaller efficiencies, W^+W^- events of other decay types and these are included by summing over the number of events of each decay type selected by selection i. The number of events of a type j selected by selection i is proportional to the efficiency (ϵ_{ij}) times the branching fractions ($\mathrm{B}_{W1}, \mathrm{B}_{W2}$) of each W producing decay type j. The expected number of background events ($\mathrm{N}_i^{\mathrm{bkg}}$) passing the W^+W^- selection i is estimated using fully simulated Monte Carlo events.

Using ten equations, one for each final state, a maximum likelihood fit is performed to extract the values of the five unknown parameters ($\sigma_{WW}, \mathrm{B}_{(W\to e\bar{\nu}_e)}, \mathrm{B}_{(W\to\mu\bar{\nu}_\mu)}, \mathrm{B}_{(W\to\tau\bar{\nu}_\tau)}, \mathrm{B}_{(W\to q\bar{q})}$). The number of unknown parameters is reduced to four by requiring that the sum of the different W branching fractions equals one (unitarity constraint).

$$\mathrm{B}_{(W\to e\bar{\nu}_e)} + \mathrm{B}_{(W\to\mu\bar{\nu}_\mu)} + \mathrm{B}_{(W\to\tau\bar{\nu}_\tau)} + \mathrm{B}_{(W\to q\bar{q})} = 1$$

In the second fit performed, values of σ_{WW}, $\mathrm{B}_{(W\to l\bar{\nu}_l)}$ and $\mathrm{B}_{(W\to q\bar{q})}$ are obtained by imposing the additional constraint of charge current lepton universality. Charge current lepton universality refers to the assumption that couplings between leptons and W are the same for all the different types of leptons. Under this assumption, the different branching fractions of the W decaying to a lepton are therefore all equal (ignoring phase space effects), i.e. $\mathrm{B}_{(W\to e\bar{\nu}_e)} = \mathrm{B}_{(W\to\mu\bar{\nu}_\mu)} = \mathrm{B}_{(W\to\tau\bar{\nu}_\tau)} \equiv \mathrm{B}_{(W\to l\bar{\nu}_l)}$. A third maximum likelihood fit is performed to find σ_{WW} alone by constraining the W branching fractions to their predicted SM values. Table 5 shows the results of each fit using data taken at 183 GeV.

The total W^+W^- cross-section at a centre-of-mass of 183 GeV is measured to be 15.43 ± 0.61(stat.) ± 0.26(sys.) pb [8] assuming SM branching fractions. This result and three other

Decay Type	Observed Number of Events	Expected Number of Events	Selection Efficiency
$W^+W^- \to e^+\nu_e e^-\bar{\nu}_e$	12	8.8±0.6	67.3%
$W^+W^- \to e^+\nu_e \mu^-\bar{\nu}_\mu$	11	17.8±0.6	69.9%
$W^+W^- \to e^+\nu_e \tau^-\bar{\nu}_\tau$	20	17.6±1.6	58.2%
$W^+W^- \to \mu^+\nu_\mu \mu^-\bar{\nu}_\mu$	13	10.7±1.0	73.7%
$W^+W^- \to \mu^+\nu_\mu \tau^-\bar{\nu}_\tau$	15	15.7±1.2	56.4%
$W^+W^- \to \tau^+\nu_\tau \tau^-\bar{\nu}_\tau$	7	8.2±0.7	44.1%
$W^+W^- \to q\bar{q}e\bar{\nu}_e$	140	129.8±3.6	84.0%
$W^+W^- \to q\bar{q}\mu\bar{\nu}_\mu$	120	123.2±2.8	86.2%
$W^+W^- \to q\bar{q}\tau\bar{\nu}_\tau$	101	118.2±3.3	64.6%
$W^+W^- \to q\bar{q}q'\bar{q}'$	438	442.6±12.4	84.6%

Table 4: Observed and expected number of events for each decay type at a centre-of-mass energy of 182.68±0.05 GeV assuming M_W = 80.40±0.09 GeV, SM W branching fractions and a calculated SM σ_{WW} of 15.72 pb. The selection efficiencies for each decay type appears in the last column.

	FIT CONSTRAINTS		
	Unitarity	Lepton Universality	SM Branching Fractions
$B_{(W\to e\bar{\nu}_e)}$	0.121±0.010±0.003		
$B_{(W\to \mu\bar{\nu}_\mu)}$	0.107±0.009±0.003		
$B_{(W\to \tau\bar{\nu}_\tau)}$	0.094±0.011±0.003		
$B_{(W\to q\bar{q})}$	0.678±0.013±0.005	0.676±0.013±0.005	
$B_{(W\to l\bar{\nu}_l)}$		0.108±0.004±0.002	
σ_{WW} (pb)	15.33±0.61±0.27	15.43±0.61±0.26	15.43±0.61±0.26

Table 5: Results of W^+W^- cross-section and branching fraction measurements extracted from a maximum likelihood fit using three different constraints described in the text. Data were taken at a centre-of-mass energy of 183 GeV. The first error is statistical and the second one is systematic.

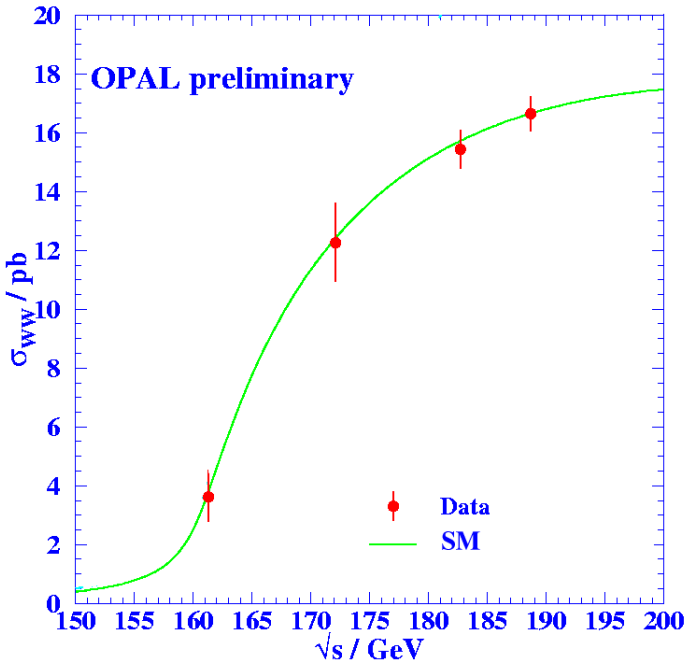

Figure 4: Plot of the total W^+W^- production cross-section versus the centre-of-mass energy ($\sqrt{s}$). The points represent the OPAL measurements and the solid line is the SM prediction for a W mass of 80.40 GeV.

W^+W^- cross-section measurements taken at different centre-of-mass energies are shown in Figure 4. The cross-section measurements appear as points with error bars and the solid line represents the SM prediction for a W mass of 80.40 GeV.

3.2 W Mass and Width

The mass of the W boson (M_W) is a key parameter in the SM. Two different methods are used at OPAL to measure the mass of the W boson depending on the energy at which W^+W^- events were produced. The W width (Γ_W), which is inversely proportional to its lifetime, is measured at LEP using data taken at a centre-of-mass energy above the W^+W^- production threshold.

3.2.1 W^+W^- events produced at threshold

Near the W^+W^- production threshold ($\sqrt{s} \sim 161$ GeV), M_W is extracted using the number of observed W^+W^- events of each decay type [9]. At this centre-of-mass energy, the W^+W^- cross-section is sensitive to the mass of the W due to the fast rise in the W^+W^- cross-section. Figure 5 shows the sensitivity of the W^+W^- cross-section to M_W where the point with error bars represents the OPAL W^+W^- cross-section measurement at a centre-of-mass of 161 GeV.

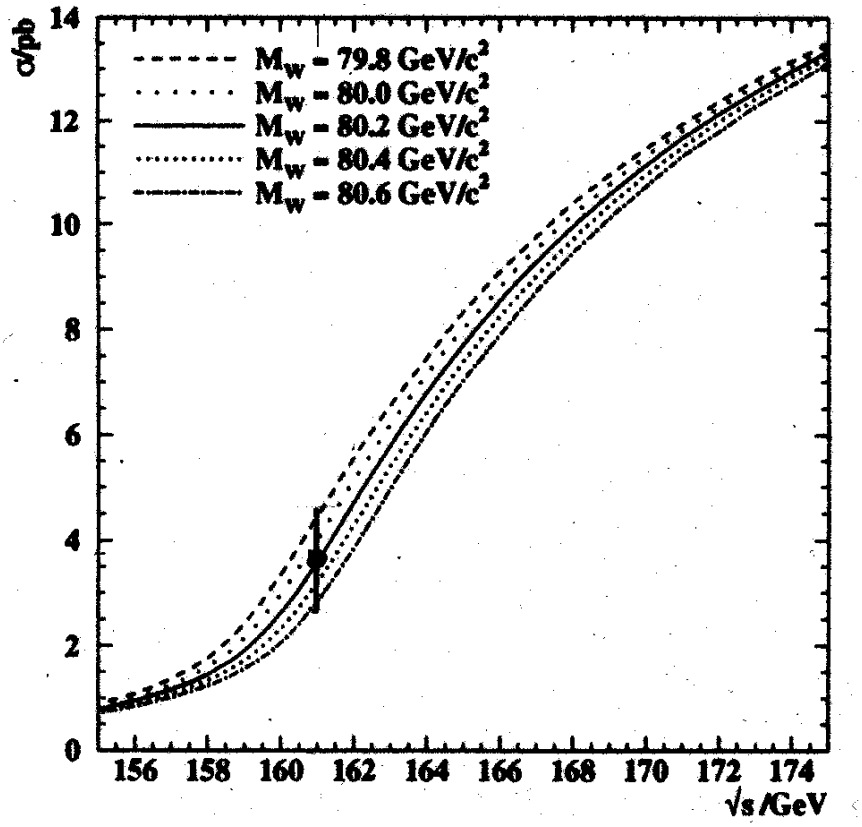

Figure 5: SM prediction of the W^+W^- production cross-section as a function of the centre-of-mass energy for different values of M_W. The OPAL W^+W^- cross-section measurement at 161 GeV appears as a point with error bars. The fast rise of the W^+W^- cross-section makes it sensitive to M_W.

The W mass is determined by comparing the number of observed and expected events of each W^+W^- decay type using a maximum likelihood fit. The expected number of W^+W^- events is obtained from Monte Carlo simulations generated at different values of M_W. The width of the W boson is constrained to its SM value.

3.2.2 W^+W^- events produced above threshold

At a centre-of-mass energy above threshold, the W mass and width are extracted by comparing the reconstructed mass distribution of the data to the mass distribution of Monte Carlo generated events at different values of M_W and Γ_W. At a centre-of-mass of 183 GeV, the reconstructed mass distributions are asymmetric due to initial state radiation. The shape of the reconstructed mass is well described by a relativistic Breit-Wigner function [10]. The fully leptonic events ($W^+W^- \to \bar{l}\nu_l l'\bar{\nu}_{l'}$) are not used in this analysis as the presence of two undetected neutrinos results in an underconstrained distribution of possible momenta.

The reconstructed invariant mass of each selected W^+W^- event is calculated by performing a kinematic fit with constraints of energy and momentum conservation. The masses of the two W candidates are also required to be equal. The kinematic fit uses a χ^2-minimization technique and the method of Lagrange multipliers. An ambiguity exists in pairing the four jets from $W^+W^- \to q\bar{q}q'\bar{q}'$ events since the flavours of the original quarks are not known. There exists three possible jet pairing combinations. A likelihood fit is performed and the combination corresponding to the largest likelihood is retained. The reconstructed invariant mass distribution for each W^+W^- decay type used in this analysis is shown in Figure 6 for data collected at 183 GeV. The theoretical prediction that best fit the data is found using a binned log-likelihood. The mass spectra of background events are assumed to be independent of M_W and Γ_W. A reweighting technique [11] is used to simulate signal events at any given W mass and width. M_W is determined by performing a one-parameter fit where Γ_W is constrained to its SM relation to the W mass. A two-parameter fit, where both M_W and Γ_W are simultaneously varied, is used to extract a value of Γ_W.

3.2.3 Results

The OPAL W mass measurement using data taken at a centre-of-mass of 161, 172 and 183 GeV is 80.38±0.12(stat.)±0.05(syst.) GeV [10]. Combining this W mass measurement with results from the other LEP experiments gives a value of 80.37±0.09 GeV where the uncertainty represents both statistical and systematic errors. As mentioned earlier, W bosons are also produced at proton-antiproton colliders. The most recent W mass measurements from the D0 and CDF collaborations at Fermilab are 80.43±0.11 [5] and 80.140±0.180 [12] where the errors include both statistical and systematic uncertainties. The width of the W boson is measured at OPAL to be 1.84±0.32(stat.)±0.20(syst.) GeV using events observed at a centre-of-mass of 172 GeV and 183 GeV [10]. The most recent D0 and CDF W width measurements are 2.044±0.097 GeV [13] where the error includes both statistical and systematic effects and 2.11±0.28(stat.)±0.16(syst.) GeV [14].

As discussed in Chapter 1, it is possible to set limits on the Higgs mass from a measurement of M_W. Figure 7 shows graphically the current constraints on M_H using measurements of the W and top quark masses. The solid red line represents the 68% confidence level (C.L.) obtained from direct measurements of the W and top quark masses. Results from indirect measurements are shown as a dotted green contour line. The diagonal yellow area represents the SM prediction for Higgs mass between 90 GeV to 1000 GeV. Current direct and indirect M_W measurements favor a light Higgs. The latest OPAL and LEP lower limits on the mass of a SM Higgs from direct searches is 88.3 GeV [15] and 89.7 GeV [16] respectively at 95% confidence level.

4 Triple Gauge Couplings

As explained in section 2, the production of W pair events involves the interaction between three bosons: γW^+W^- and $Z^0W^+W^-$. Triple gauge couplings (TGCs) exist since the measured W^+W^- cross-section shown in Figure 8 agrees with the SM prediction. The form

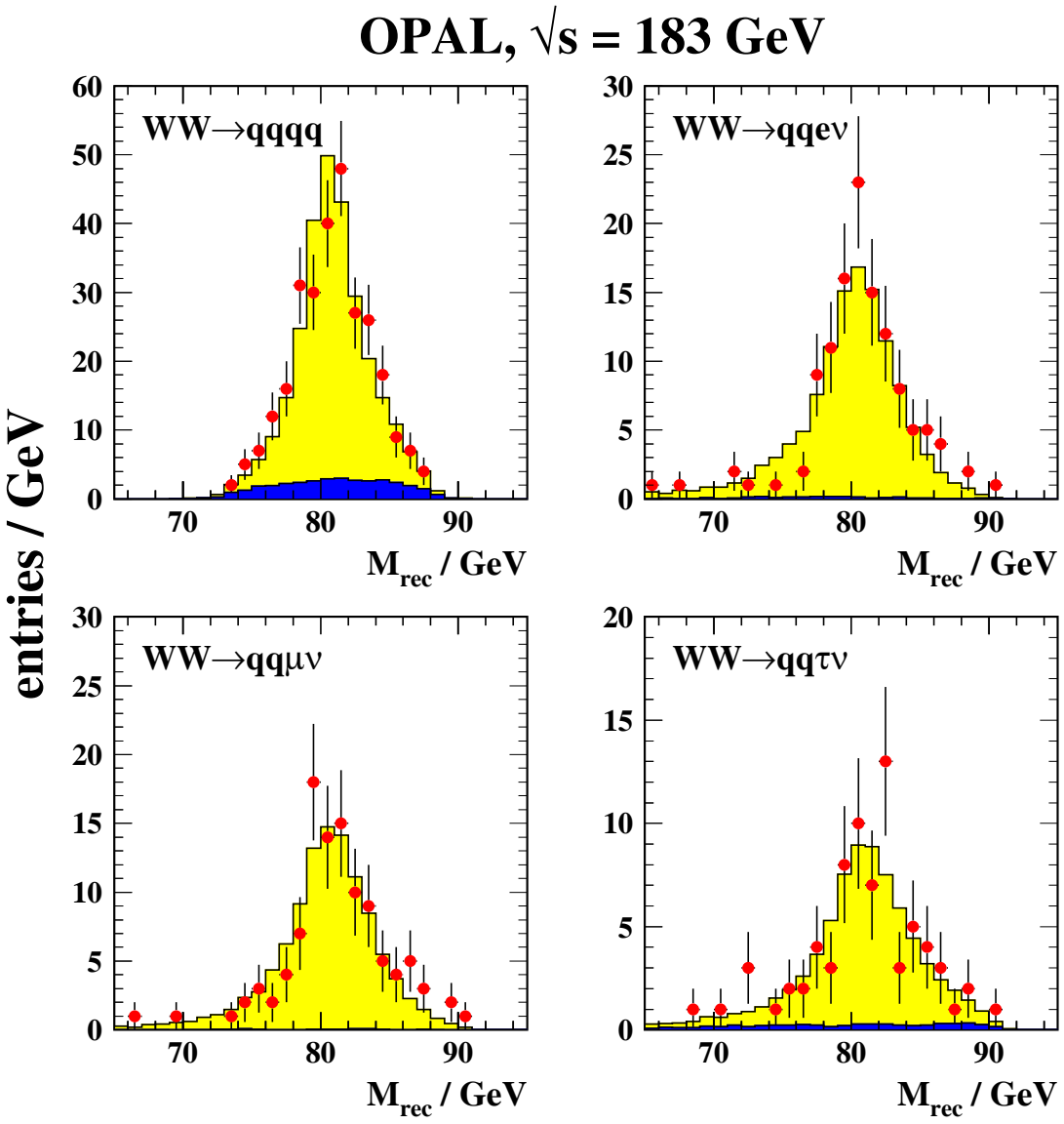

Figure 6: Reconstructed W mass distributions for $W^+W^- \to q\bar{q}q'\bar{q}'$, $W^+W^- \to q\bar{q}e\bar{\nu}_e$, $W^+W^- \to q\bar{q}\mu\bar{\nu}_\mu$ and $W^+W^- \to q\bar{q}\tau\bar{\nu}_\tau$ events. The points corresponds to data taken at 183 GeV and the yellow histograms show the results of the fitted mass. The blue histograms represent the background contribution.

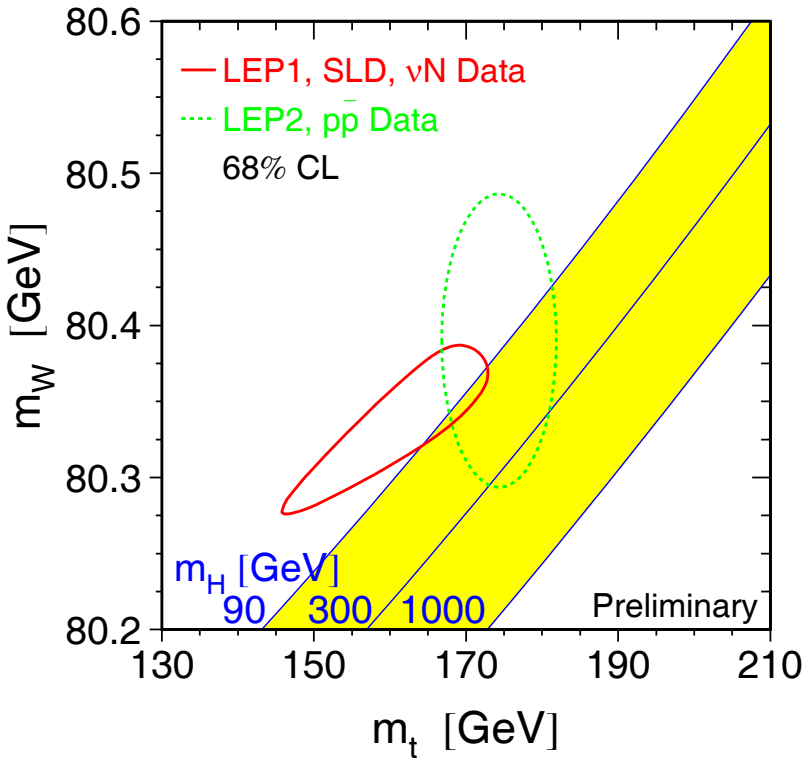

Figure 7: Plot of the measured M_W versus the top quark mass. The diagonal yellow band represents the SM prediction for Higgs mass between 90 to 1000 GeV. The solid red (dotted green) ellipse represents the 68% confidence level contour from indirect (direct) M_W measurements. Current M_W measurements seem to favor a light Higgs.

of the TGCs might however be different from what the SM predicts. A brief theoretical introduction to TGCs is presented in the following paragraphs in order to explain the basic formalism used in the experimental measurement of these couplings.

4.1 TGC Lagrangian

In quantum field theory, particles are described as quantized excitations of different fields. The dynamics of these fields can be expressed mathematically in terms of a function $\mathcal{L}$ called a Lagrangian density [11].

The most general Lagrangian density describing the interaction between two charged bosons (W^+,W^-) and a neutral gauge boson (Z^0 or γ) can be written as

$$\begin{aligned} i\mathcal{L}^{WWV}/g_{WWV} &= \boldsymbol{g_1^V} V^\mu (W^-_{\mu\nu} W^{+\nu} - W^+_{\mu\nu} W^{-\nu}) \\ &+ \boldsymbol{\kappa_V} W^+_\mu W^-_\nu V^{\mu\nu} \end{aligned}$$

[11] The Lagrangian L is defined as $L = \int \mathcal{L} dx^3$

$$
\begin{aligned}
&+ \quad \frac{\boldsymbol{\lambda_V}}{m_W^2} V^{\mu\nu} W_\nu^{+\rho} W_{\rho\mu}^- \\
&+ \quad i\boldsymbol{g_5^V} \varepsilon_{\mu\nu\rho\sigma} [(\partial^\rho W^{-\mu}) W^{+\nu} - W^{-\mu} (\partial^\rho W^{+\nu})] V^\sigma \\
&+ \quad i\boldsymbol{g_4^V} W_\mu^- W_\nu^+ (\partial^\mu V^\nu + \partial^\nu V^\mu) \\
&- \quad \frac{\boldsymbol{\tilde{\kappa}_V}}{2} W_\mu^- W_\nu^+ \varepsilon^{\mu\nu\rho\sigma} V_{\rho\sigma} \\
&- \quad \frac{\boldsymbol{\tilde{\lambda}_V}}{2m_W^2} W_{\rho\mu}^- W_\nu^{+\mu} \varepsilon^{\nu\rho\alpha\beta} V_{\alpha\beta} \qquad (1)
\end{aligned}
$$

where V^μ represents the four-vector potential of either a photon (γ) or a Z^0 boson. $W^{+\mu}$ and $W^{-\mu}$ correspond to the fields associated with the W^+ and W^- boson respectively. Also, $W_{\mu\nu} = \partial_\mu W_\nu - \partial_\nu W_\mu$ and similarly, $V_{\mu\nu} = \partial_\mu V_\nu - \partial_\nu V_\mu$. The totally antisymmetric[12] symbol $\varepsilon^{\mu\nu\rho\sigma}$ is defined as $\varepsilon^{0123} = 1$. TGCs appear in equation 1 in bold font. Theoretically, there exists a total of seven different combinations (corresponding to the seven terms in the Lagrangian density) through which a pair of W bosons can interact with a neutral boson. In the SM, $g_1^Z = g_1^\gamma = \kappa_\gamma = \kappa_Z = 1$ and all the other couplings are zero. Anomalous TGCs refer to values of couplings that are different from the SM prediction. Table 6 lists the symmetry properties of each term of the Lagrangian density under charge conjugation[13]($\mathcal{C}$) and parity transformation[14]($\mathcal{P}$).

	Conserve		
	$\mathcal{C}$	$\mathcal{P}$	$\mathcal{CP}$
g_1^V	×	×	×
κ_V	×	×	×
λ_V	×	×	×
g_5^V			×
g_4^V		×	
$\tilde{\kappa}_V$	×		
$\tilde{\lambda}_V$	×		

Table 6: Symmetry properties of each term of the Lagrangian density under charge conjugation, $\mathcal{C}$, and parity, $\mathcal{P}$. The subscript V stands for γ or Z^0. The only non-zero couplings in the SM ($g_1^Z, g_1^\gamma, \kappa_\gamma, \kappa_Z$) conserve both $\mathcal{C}$ and $\mathcal{P}$.

Terms in equation 1 describing $\gamma W^+ W^-$ vertices can be associated with a classical multipole expansion of the W γ interactions. The electric charge (Q_W), electric and magnetic

[12]The interchange of any two indices brings a minus sign and the symbol has a value of zero if any two indices are the same.

[13]The charge conjugation operator, $\mathcal{C}$, converts each particle into its antiparticle.

[14]The parity operator, $\mathcal{P}$, inverts spatial coordinates such that x→ -x, y → -y and z → -z.

dipole moments (d_W, μ_W) and electric and magnetic quadrupole moments (q_W, $\tilde{Q}_W$) of the W can then be written in terms of TGCs.

$$
\begin{aligned}
Q_W &= e g_1^\gamma && (2)\\
d_W &= \frac{e}{2m_W}(\tilde{\kappa}_\gamma + \tilde{\lambda}_\gamma) && (3)\\
\mu_W &= \frac{e}{2m_W}(g_1^\gamma + \kappa_\gamma + \lambda_\gamma) && (4)\\
q_W &= -\frac{e}{m_W^2}(\kappa_\gamma - \lambda_\gamma) && (5)\\
\tilde{Q}_W &= -\frac{e}{m_W^2}(\tilde{\kappa}_\gamma - \tilde{\lambda}_\gamma) && (6)
\end{aligned}
$$

With this physical interpretation in mind, the existence of anomalous couplings could indicate that the W is a composite particle.

In order to experimentally measure TGCs, all fourteen couplings in equation 1 should be taken as free parameters to be fitted to data. This is, however, impossible to do with the amount of data available. To reduce the number of free parameters, the interaction between three gauge bosons is assumed to conserve $\mathcal{C}$, $\mathcal{P}$ and be electromagnetic gauge invariant. Five parameters are left ($g_1^Z, \kappa_Z, \kappa_\gamma, \lambda_Z$ and λ_γ). The requirement that the Lagrangian density be SU(2)$\otimes$U(1) gauge invariant and precise measurements at lower energy further constrain this set of parameters with the following relations [17],

$$
\begin{aligned}
\Delta\kappa_Z &= -\Delta\kappa_\gamma \tan^2\theta_w + \Delta g_1^Z && (7)\\
\lambda_Z &= \lambda_\gamma && (8)
\end{aligned}
$$

where Δ indicates deviations of the couplings from their SM values and θ_w is the weak mixing angle. This reduces the set of couplings to only three free parameters which are chosen by convention to be $\Delta\kappa_\gamma, \Delta g_1^Z$ and λ ($\lambda = \lambda_Z = \lambda_\gamma$).

4.2 Effects of Anomalous TGCs

Pairs of W boson can be produced in nine different helicity[15] states. Anomalous TGCs affect the total W^+W^- cross-section as well as the W angular distribution by changing the fraction of W^+W^- produced in each helicity state. The angular distributions of the W decay products are also affected because they depend on the W helicity state.

Figure 8 is a plot of the W^+W^- cross-section as a function of the centre-of-mass energy. The solid line is the SM prediction and the dashed line is the expected cross-section calculated without $Z^0W^+W^-$ interactions which corresponds to anomalous couplings $\Delta\kappa_\gamma = 0$, $\Delta g_1^Z = -1$, $\lambda = 0$. The data are in good agreement with the SM prediction which suggests that large values of anomalous couplings are not likely to exist.

[15]The helicity of a particle is defined as the projection of its spin onto its direction of motion. Each W boson can have helicity +1,0 and -1.

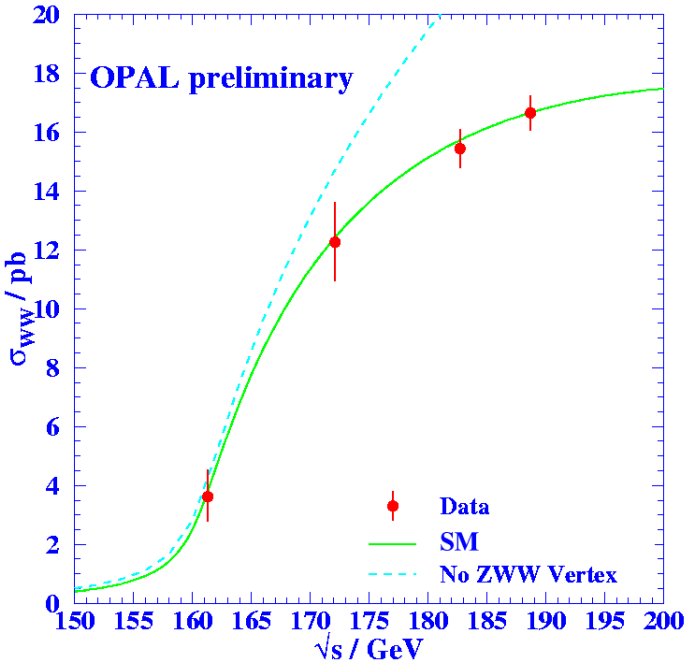

Figure 8: Plot of the total W^+W^- production cross-section as a function of the centre-of-mass energy ($\sqrt{s}$). The points are data and the solid line represents the SM prediction ($\Delta\kappa_\gamma = 0$, $\Delta g_1^Z = 0$, $\lambda = 0$). The dashed line corresponds to the case with no $Z^0W^+W^-$ interactions ($\Delta\kappa_\gamma = 0$, $\Delta g_1^Z = -1$, $\lambda = 0$).

In the approximation of small W width and no initial state radiation, each W^+W^- event can be characterised by five angles. By convention, these angles are taken to be the W production angle θ_W with respect to the electron beam and the polar (θ^*) and azimuthal (ϕ^*) angles of the decay products of each W in the W rest frame.

The five angles of leptonically decaying W^+W^- events ($W^+W^- \to \bar{l}\nu_l l'\bar{\nu}_{l'}$) can only be reconstructed in the approximation of zero W width and no initial state radiation for $l = e$ or μ. The kinematic angles of the event cannot be reconstructed if one of the W decays to a τ since a third undetected neutrino is produced when the τ decays. Using the charge and momenta of the two observed leptons, a kinematic fit is performed to find the values of the five angles. Each lepton-neutrino pair is constrained to have a reconstructed mass equal to the mass of the W . Furthermore, the two W bosons are also assumed to recoil back-to-back in the lab frame with a total energy equal to the centre-of-mass energy.

For $W^+W^- \to q\bar{q}\bar{l}\nu_l$ events, the W production angle θ_W is obtained by summing the four-momenta of the two jets. The decay angles of the charged lepton (θ_l^*, ϕ_l^*) are obtained from the four-momentum of the lepton boosted back to the W rest frame. The charge of the identified lepton determines the charge of the parent W . For the hadronically decaying W , an ambiguity exists in assigning each jet to the primary quark or antiquark. This ambiguity is taken into account when extracting values of TGCs.

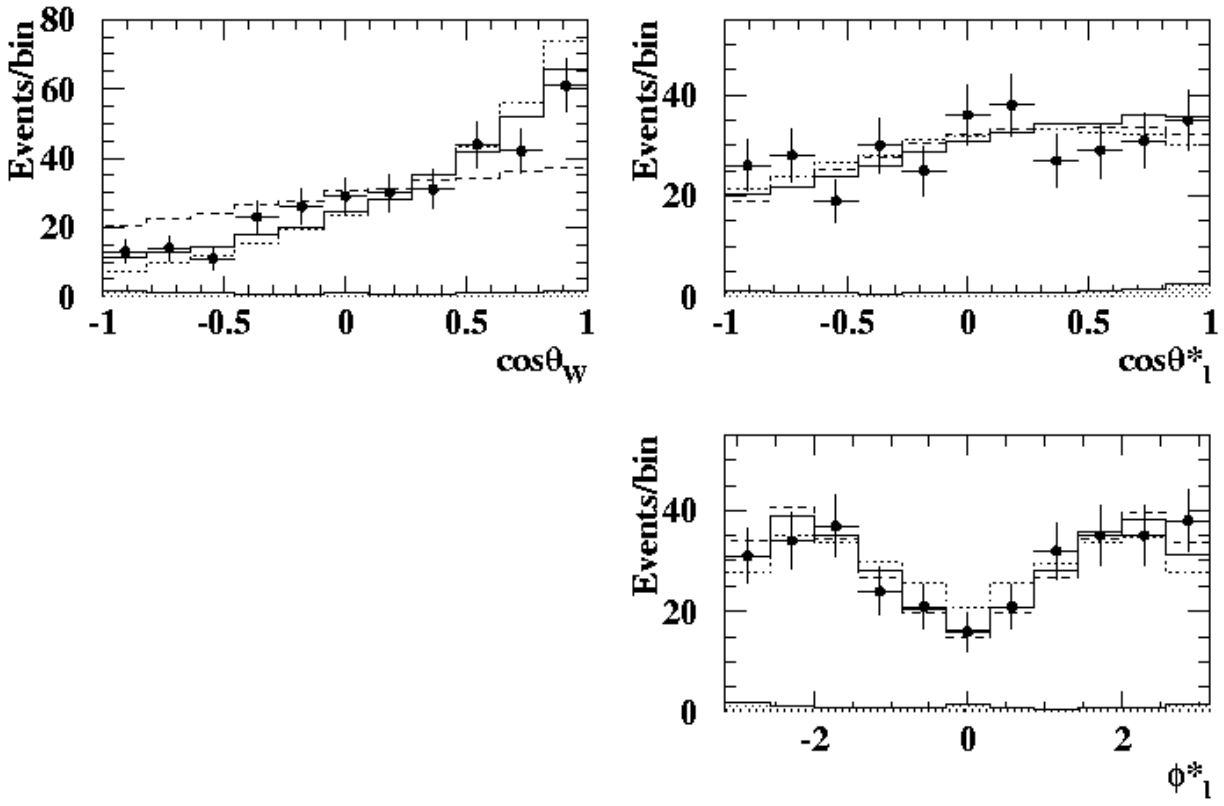

Figure 9: Angular distributions of W bosons (θ_W) and W decay products in the W rest frame (θ_l^*, ϕ_l^*) for $W^+W^- \to q\bar{q}\bar{l}\nu_l$ events at 183 GeV. The points are data and the solid histograms represent the SM prediction. The distributions expected in the case $\Delta g_1^Z = +1$(-1) are shown as dotted (dashed) histograms. The other two anomalous couplings are set to zero ($\Delta\kappa_\gamma = 0$, $\lambda = 0$). Background events are represented by the filled dotted histograms.

In a fully hadronic W^+W^- event ($W^+W^- \to q\bar{q}q'\bar{q}'$), there exists three jet pairing possibilities. The most likely combination is chosen by a likelihood algorithm. Once one jet pairing combination is chosen, the W^- is identified to belong to the pair of jets whose charge is more negative. Most of the sensitivity to TGCs is contained in the W production angle θ_W due to the lack of separation between quark and antiquark jets.

The effects of anomalous couplings on the angular distributions of the W and the W decay products of $W^+W^- \to q\bar{q}\bar{l}\nu_l$ events are shown in Figure 9. The solid points indicate the 183 GeV data and the solid line histograms represent the SM prediction. The dotted and dashed histograms represent the theoretical prediction corresponding to anomalous couplings $\Delta g_1^Z = +1$ and -1 respectively ($\Delta\kappa_\gamma = 0$, $\lambda = 0$). It is interesting to note that W bosons are mainly produced forward due to the presence of the neutrino exchange diagram [17] (see Figure 1).

Different statistical techniques are used to extract TGCs from experimental data [8, 17].

It is beyond the scope of this report to describe and discuss the different methods. Combining data taken at different centre-of-mass energies (161, 172 and 183 GeV) from all W decay final states, TGCs are measured to be [8]

$$\Delta\kappa_\gamma = +0.1^{+0.52}_{-0.37} \qquad \Delta g_1^Z = +0.01^{+0.13}_{-0.12} \qquad \lambda = -0.10^{+0.13}_{-0.12}$$

where the uncertainties include both statistical and systematic errors. These results are all consistent with the SM values of zero.

5 Summary

The study of W^+W^- events provides important information on the SM and a chance to search for possible new physics effects. The mechanisms by which W pairs are produced and identified in the OPAL detector have been presented. The methods used to extract the W^+W^- cross-section and the W decay branching fractions have been summarized. The importance of the W mass measurement has been discussed as well as the two different methods used to extract this measurement. Finally, an introduction to TGCs was presented with the latest measurements from the OPAL Collaboration. Data are consistent with the SM predictions. Search for possible new physics will continue at higher energies (up to 200 GeV) in the next two years left of LEP running.

References

[1] I. J. R. Aitchison, Gauge Theories in Particle Physics, Adam Hilger (1989).

[2] The UA1 Collaboration, G. Arnison *et al.*, Phys. Lett. **122B** (1983) 103.
The UA2 Collaboration, M. Banner *et al.*, Phys. Lett. **122B** (1983) 476-485.

[3] Particle Data Group, C. Caso *et al.*, Eur. Phys. J. **C3**, (1998) 19.

[4] P. Renton, Electroweak Interactions:An Introduction to the Physics of Quarks and Leptons, Cambridge University Press (1990) 535.

[5] The D0 Collaboration, B. Abbott *et al.*, Phys. Rev. **D58** (1998) 092003.

[6] A. Sirlin, Phys. Rev. **D22** (1980) 971; W. Marciano and A. Sirlin, Phys. Rev. **D22** (1980) 2695 and erratum-ibid **D31** (1985) 213.

[7] The OPAL Collaboration, K. Ahmet *et al.*, Nucl. Instr. Meth. **A305** (1991) 275.

[8] The OPAL Collaboration, K. Ackerstaff et al., CERN-EP/98-167 (1998).

[9] The OPAL Collaboration, K. Ackerstaff *et al.*, Phys. Lett. **B389** (1996) 416-428.

[10] The OPAL Collaboration, G. Abbiendi *et al.*, CERN-EP/98-197 (1998).

[11] The OPAL Collaboration, K. Ackerstaff *et al.*, CERN-PPE/97-116 (1997).

[12] The CDF Collaboration, F. Abe *et al.*, Phys. Rev. **D52** 4784 (1995).

[13] The D0 Collaboration, B. Abbott *et al.*, FERMILAB-PUB-99-015-E, submitted to Phys. Rev. **D**.

[14] The CDF Collaboration, F. Abe *et al.*, Phys. Rev. Lett. **74** (1995) 341.

[15] The OPAL Collaboration, G. Abbiendi *et al.*, Eur. Phys. J. **C7** (1999) 407.

[16] The LEP Working Group for Higgs Boson Searches, The ALEPH, DELPHI, L3 and OPAL Collaborations, CERN-EP/99-060 (1999).

[17] Proceedings of CERN LEP2 Workshop, CERN 96-01, Vols. 1 and 2, eds. G. Altarelli, T. Sjöstrand and F. Zwirner, February 1996.